Fukushima *et al. Earth, Planets and Space* (2017) 69:112
DOI 10.1186/s40623-017-0698-z

Earth, Planets and Space

FULL PAPER

Open Access

Geomagnetically conjugate observations of ionospheric and thermospheric variations accompanied by a midnight brightness wave at low latitudes

D. Fukushima[1,5], K. Shiokawa[1*], Y. Otsuka[1], M. Kubota[2], T. Yokoyama[2], M. Nishioka[2], S. Komonjinda[3] and C. Y. Yatini[4]

Abstract

We conducted geomagnetically conjugate observations of 630-nm airglow for a midnight brightness wave (MBW) at Kototabang, Indonesia [geomagnetic latitude (MLAT): 10.0°S], and Chiang Mai, Thailand (MLAT: 8.9°N), which are geomagnetically conjugate points at low latitudes. An airglow enhancement that was considered to be an MBW was observed in OI (630-nm) airglow images at Kototabang around local midnight from 2240 to 2430 LT on February 7, 2011. This MBW propagated south-southwestward, which is geomagnetically poleward, at a velocity of 290 m/s. However, a similar wave was not observed in the 630-nm airglow images at Chiang Mai. This is the first evidence of an MBW that does not have geomagnetic conjugacy, which also implies generation of MBW only in one side of the hemisphere from the equator. We simultaneously observed thermospheric neutral winds observed by a co-located Fabry–Perot interferometer at Kototabang. The observed meridional winds turned from northward (geomagnetically equatorward) to southward (geomagnetically poleward) just before the wave was observed. This indicates that the observed MBW was generated by the poleward winds which push ionospheric plasma down along geomagnetic field lines, thereby increasing the 630-nm airglow intensity. The bottomside ionospheric heights observed by ionosondes rapidly decreased at Kototabang and slightly increased at Chiang Mai. We suggest that the polarization electric field inside the observed MBW is projected to the northern hemisphere, causing the small height increase observed at Chiang Mai. This implies that electromagnetic coupling between hemispheres can occur even though the original disturbance is caused purely by the neutral wind.

Introduction

OI (630-nm) airglow imaging has been widely used to observe ionospheric disturbances since the development of highly sensitive back-illuminated cooled charge-coupled devices (CCDs). The 630-nm airglow emission layer is located at altitudes of ~200–300 km at the bottom of the ionospheric F region. The dominant process of the 630-nm airglow emission is the chemical reaction of oxygen ions (O^+) with molecular oxygen (O_2) (e.g., Sobral et al. 1993). The airglow intensity is proportional to the product of the densities of O^+ and O_2. Because the O^+ density is almost the same as the electron density in the F region, 630-nm airglow is a sensitive indicator of F-region plasma density. The 630-nm airglow intensity increases when the F-region height decreases, because the O^+ reacts with high-density O_2 at lower altitudes. Thus, 630-nm airglow is also sensitive to F-region height variations.

Brightness waves are a phenomenon in which a region of 630-nm airglow enhancement propagates in the meridional directions at low latitudes. Thus, the brightness waves are a type of large-scale traveling ionospheric disturbances (LSTIDs) which have a horizontal scale

*Correspondence: shiokawa@nagoya-u.jp
[1] Institute for Space-Earth Environmental Research, Nagoya University, Nagoya, Aichi 464-8601, Japan
Full list of author information is available at the end of the article

size of more than 1000 km (e.g., Hunsucker 1982). The first observations of a brightness wave were recorded by Greenspan (1966) and Nelson and Cogger (1971) in the American longitudinal sector. Colerico et al. (1996) observed several brightness wave events by using an all-sky imager at Arequipa, Peru. Brightness waves were observed in the pre-midnight sector (~20–22 LT) and midnight sector (~23–01 LT). The earlier brightness wave in that observation propagated northward (equatorward) and the later brightness wave propagated southward (poleward), typically as a single pulse of 630-nm airglow enhancement. They called these waves the pre-midnight brightness wave (PMBW) and the midnight brightness wave (MBW), respectively. For these brightness wave events, they observed thermospheric neutral winds and temperature by a Fabry–Perot interferometer (FPI) and ionospheric heights by an ionosonde. For each instance, the FPI data showed a local minimum in zonal wind and a reversal in meridional winds, from equatorward to poleward, and the ionosonde data showed a height decrease in the F region. The observed neutral temperature showed a local maximum which is considered to be the midnight temperature maximum (MTM) (e.g., Mayr et al. 1979). The MTM tends to have larger amplitude during the local summer months (e.g., Martinis et al. 2013). Colerico et al. (1996) suggested that a pressure bulge accompanying the MTM reverses the meridional winds from equatorward to poleward; therefore, the poleward winds move the F region to lower altitudes along the geomagnetic field, enhancing the 630-nm airglow intensity as the MBW. The other MBW observations were conducted at Arecibo, Puerto Rico (Mendillo et al. 1997), and Shigaraki, Japan (Otsuka et al. 2003). The characteristics of these observed MBWs were similar to those reported by Colerico et al. (1996). However, the apparent phase velocity of the MBW observed in Japan (~500 m/s) was larger than that observed in Peru (~250–350 m/s) and Puerto Rico (~300 m/s). If the MTM pressure bulge generates MBWs, the MBWs can be launched toward both the northern and southern hemispheres. If the MBWs are purely neutral phenomena, there would be no geomagnetic conjugacy of the ionospheric and thermospheric signatures associated with the MBWs. However, there have been no attempts to make simultaneous observations of MBWs at northern and southern hemispheres.

Since 1998, the Solar-Terrestrial Environment Laboratory (STEL) [currently the Institute for Space-Earth Environmental Research (ISEE)] at Nagoya University has developed a series of all-sky airglow imagers as the Optical Mesosphere Thermosphere Images (OMTIs) (Shiokawa et al. 1999, 2009). Recent airglow observations have been used to investigate nighttime medium-scale traveling ionospheric disturbances (MSTIDs) from low to high latitudes (e.g., Fukushima et al. 2012; Shiokawa et al. 2012a) and plasma bubbles at equatorial and middle latitudes (e.g., Shiokawa et al. 2004; Fukushima et al. 2015). Otsuka et al. (2002, 2004) conducted nighttime airglow observations with all-sky imagers at middle-latitude geomagnetically conjugate points in Japan and Australia for plasma bubbles and MSTIDs, respectively. They found that the plasma bubbles and nighttime MSTIDs had symmetrical structures in both hemispheres and were connected by geomagnetic field lines. These observations indicate that the electric fields in the F region play an important role in creating the observed ionospheric disturbances. In contrast, this type of conjugate observation has not been conducted for the MBWs.

In this paper, we investigate the geomagnetic conjugacy of a MBW by using nighttime 630-nm airglow observations at two geomagnetically conjugate points at low latitudes. These are the first observations of MBW at geomagnetically conjugate points. We also investigate variations in thermospheric neutral winds and ionospheric heights accompanying the MBW, using an FPI and ionosondes at each conjugate point, to investigate geomagnetic conjugacy of the ionospheric and thermospheric signatures associated with the MBW.

Observations

We observed nighttime 630-nm airglow by using a highly sensitive all-sky imager (#13) at Kototabang, Indonesia [geographic latitude (GLAT): 0.2°S; geographic longitude (GLON): 100.3°E; and geomagnetic latitude (MLAT): 10.0°S]. The location of Kototabang is shown by the red point in Fig. 1. The local time of Kototabang is 7 h ahead of UT. Imager #13 is one of the OMTIs operated by STEL/ISEE (Shiokawa et al. 1999, 2009). The imager uses a cooled CCD camera which is cooled to a temperature of less than −50 °C. To observe thermospheric and ionospheric structures, we used an interference filter with a bandwidth of 1.57 nm to admit 630.0-nm (OI) emissions. The 630-nm airglow images were obtained with an exposure time of 165 s and a time resolution of 330 s at a spatial resolution of 512 × 512 CCD pixels, giving a minimum spatial resolution of less than 2 km around the zenith of the images.

Airglow observation was also conducted in Chiang Mai, Thailand (GLAT: 18.8°N; GLON: 98.9°E; and MLAT: 8.9°N). The location of Chiang Mai is shown by the blue point in Fig. 1. The local time of Chiang Mai is 7 h ahead of UT. The geomagnetically conjugate point of Kototabang, calculated by using the International Geomagnetic Reference Field (IGRF) (Finlay et al. 2010), is located ~ 3° south of Chiang Mai, as shown in Fig. 1. The Chiang Mai airglow imager is operated by the National Institute

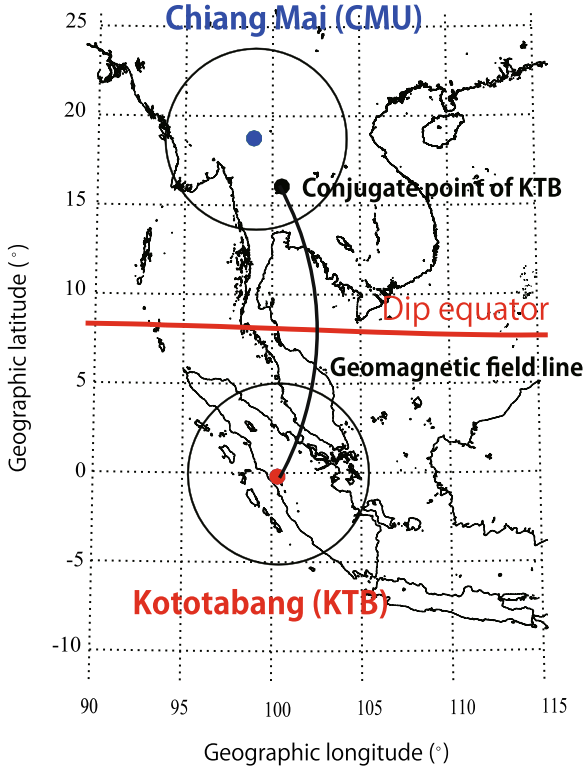

Fig. 1 Location of Kototabang (KTB) and Chiang Mai (CMU). The geomagnetically conjugate point of Kototabang is shown by the *black dot*. The *circles* show the field of view of the all-sky imagers at KTB and CMU

of Information and Communications Technology (NICT) under the Southeast Asia Low-latitude Ionospheric Network (SEALION) project (Yamamoto et al. 2002; Kubota et al. 2009). The 630-nm airglow images at Chiang Mai were obtained with an exposure time of 45 s and a time resolution of 360 s at a spatial resolution of 512 × 512 CCD pixels.

Due to the tropical climate in both Kototabang and Chiang Mai, it is very difficult to obtain simultaneous clear-sky nights from these pair stations. Particularly, the clear-sky rate of Kototabang is less than 10% of the whole observation interval. Thus, the present event is a unique event that we have clear skies at both stations and observe an MBW.

Figure 2a–d and e–h shows the 630-nm all-sky images acquired by the imagers at Kototabang and Chiang Mai, respectively, from 1602 to 1732 UT (from 2302 to 0032 LT) on February 7, 2011. The radius of the field of view of the imager is ~500 km assuming an airglow height of 250 km, and this is shown by black circles in Fig. 1. As shown in Fig. 2b, c, the airglow intensity is increased from 1632 to 1702 UT at Kototabang. However, such enhancement was not seen in the images of Chiang Mai, as shown in Fig. 2e–h. The enhanced airglow in the eastern and southern edges in Fig. 2e–h is caused by city lights, which come from the eastern edge and are reflected by the dome of the co-located FPI at the southern edge.

Figure 3a–h shows the 630-nm airglow images at Kototabang; the coordinates are converted into geographic coordinates from all-sky coordinates. For the coordinate conversion, we assume that the 630-nm airglow emission layer is located at an altitude of 250 km. Note that, in the figure, left is west and up is north, which is zonally opposite to Fig. 2. The airglow intensity is represented as the absolute value in units of Rayleigh (R), which is obtained by subtracting the background continuum emission measured at a wavelength of 572.5 nm (Shiokawa et al. 2000, 2009). Between 1548 and 1618 UT, the airglow intensity in the northeast of Kototabang (longitudes of 100–105°E and latitudes of 1°S–3°N) increased to ~400 R. Then, a wave structure with a phase front elongated from west-northwest (WNW) to east-southeast (ESE) was seen between 1632 and 1718 UT. This enhanced airglow structure is identified as an MBW because it propagated geomagnetically poleward only once, at around local midnight (e.g., Colerico et al. 1996). This MBW appeared to propagate from the zenith to the southwestern edge of the images. The airglow intensity inside the MBW was 200–600 R.

Figure 4a–h shows the 630-nm airglow images at Chiang Mai, with geographic coordinates converted from all-sky coordinates. The format is the same as in Fig. 3, although the airglow intensity is represented as the raw CCD counts because the absolute intensity could not be calculated for the data from Chiang Mai due to city-light contamination, as described below. The high airglow intensity in the eastern and southern edges of the images is due to the city-light contamination. The airglow intensity was less than 20,000 counts and was stable in the eight panels of Fig. 4, with no discernible wave structures.

In Fig. 4 we could not estimate the absolute intensity of 630-nm airglow. To calculate the absolute intensity, we need to subtract the background continuum emission which is measured at a wavelength of 572.5 nm. This procedure contains an assumption that the intensity of background continuum emission including city lights is the same at 572.5 and at 630.0 nm. However, at Chiang Mai, the subtraction of background continuum emission resulted in negative value of 630.0-nm airglow intensity. This fact suggests that the assumption of the same intensity of background continuum emission at 572.5 and 630.0 nm may be not correct. If contamination of scattered city lights contributes to the background continuum emission, this spectral dependence would occur above Chiang Mai. Since we do not measure the intensity of background continuum emission at wavelengths near

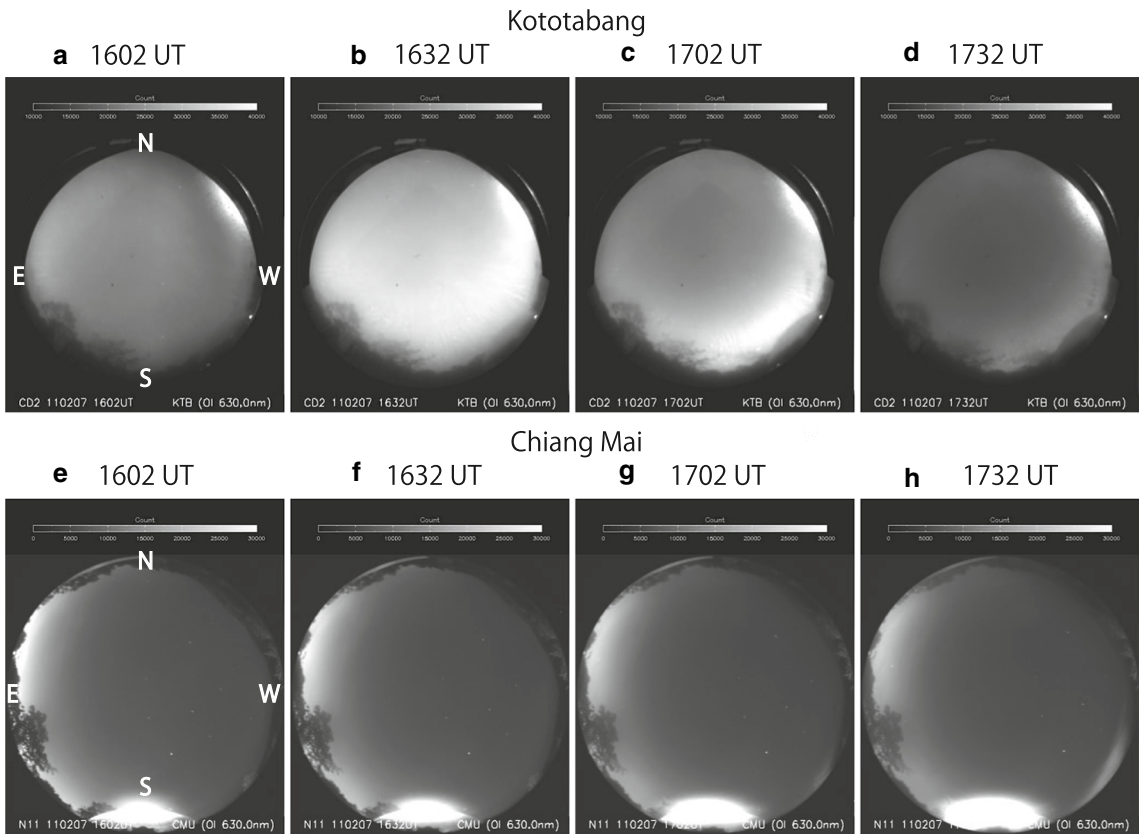

Fig. 2 All-sky images obtained by airglow imagers at **a**–**d** Kototabang and **e**–**h** Chiang Mai from 1602 to 1732 UT on February 7, 2011. Up is geographic north and left is geographic east in each image

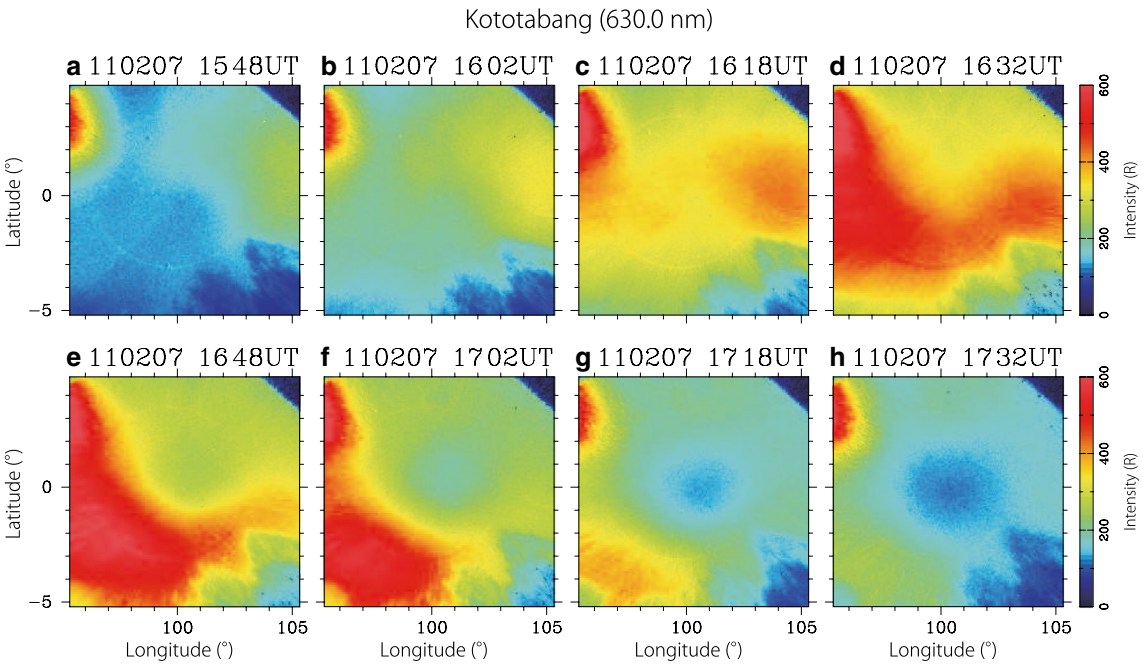

Fig. 3 Two-dimensional 630-nm airglow images from 1548 to 1732 UT on February 7, 2011, at Kototabang represented as absolute airglow intensity (R). These images are converted from all-sky coordinates to geographic coordinates

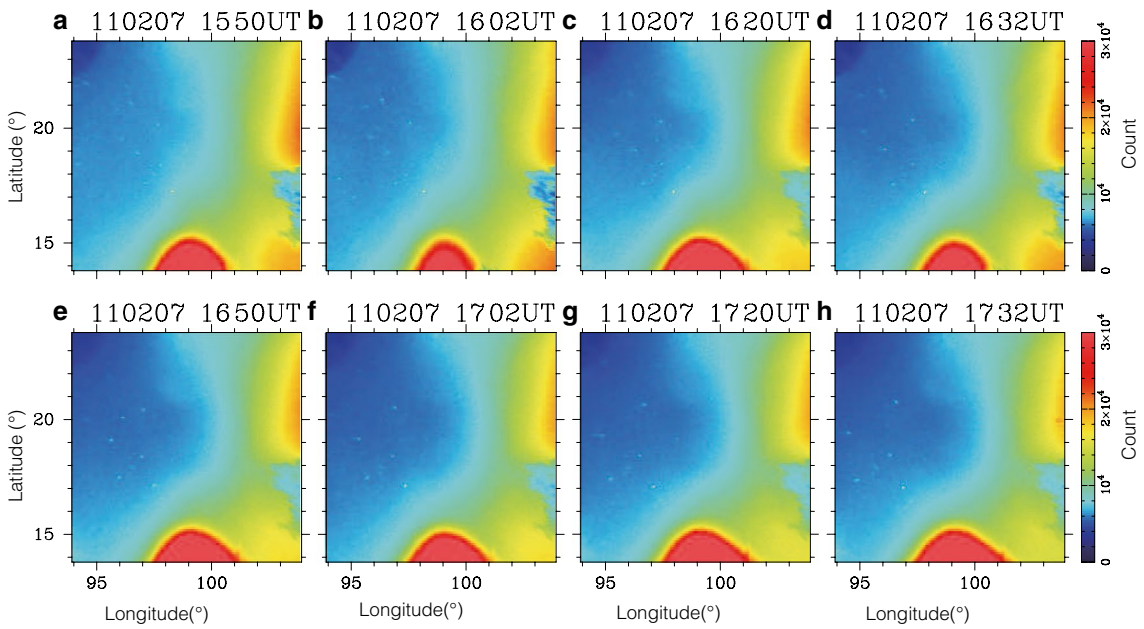

Fig. 4 Two-dimensional 630-nm airglow images from 1550 to 1732 UT on February 7, 2011, at Chiang Mai represented as raw CCD counts. These images are converted from all-sky coordinates to geographic coordinates

630.0 nm, we could not estimate the absolute intensity of the 630.0-nm airglow emission. Because the output count of CCD is proportional to the 630.0-nm airglow intensity, and because the read-out noise of the CCD is less than 10 counts (rms), which corresponds to the 630.0-nm intensity of less than 0.3 R, we can identify variations of 630-nm airglow intensity of more than 0.3 R in the imager in Chiang Mai from these raw count images in Fig. 4. Thus, we conclude that there are no discernible wave structures at Chiang Mai in the plotted interval.

To estimate the observed wave velocity, we took zonal and meridional cross sections (keograms) of the 630-nm airglow images at a fixed latitude and longitude where the wave was clearly seen. Figure 5a, b shows meridional and zonal keograms, respectively, of Kototabang at a longitude of 97.0°E and a latitude of 3.0°S (defined as point A) on February 7, 2011. A southward-moving structure with intensities of 200–600 R was seen from 1540 to 1730 UT (Fig. 5a), indicating the passage of an MBW. This MBW structure also moved slightly westward (Fig. 5b). This can be attributed to the slightly tilted phase front of MBW elongated from west-northwest (WNW) to east-southeast (ESE), as shown in Fig. 3. From these keograms and images, we conclude that the propagation direction of the wave was south-southwestward. The horizontal velocity of the MBW was ~290 m/s. The north–south scale size of this MBW seems to be more than 1000 km.

Figure 6a, b shows meridional and zonal keograms, respectively, of Chiang Mai at a longitude of 96.6°E and a latitude of 18.9°N on February 7, 2011. These latitude and longitude are the conjugate of point A. Note that the airglow intensity is represented as the raw CCD counts, as in Fig. 4. The moving structures are not seen in Fig. 6a, b, indicating that the conjugate MBW was not observed at Chiang Mai on this night. The airglow intensity above 101°E in Fig. 6b is more than 10,000 counts due to the city light.

At Kototabang and Chiang Mai, thermospheric neutral winds have been observed by co-located FPIs since 2010. These FPIs (FP03 in Kototabang and FP02 in Chiang Mai) are also a part of the OMTIs operated by STEL/ISEE (Shiokawa et al. 2012b). These FPIs use a 70-mm-diameter etalon, an interference filter that admits the 630-nm wavelength with a bandwidth of 2.5 nm, and a CCD water-cooled to a temperature of −80 °C. There is a sky scanner on top of the FPI, which sequentially scans north, south, east, and west with an exposure time of 3.5 min for each direction. We measure the meridional (zonal) wind velocity in the thermosphere by measuring the difference in the Doppler shift of the 630-nm airglow emission line through interference fringes between north and south (east and west). The time resolution for obtaining a meridional and zonal wind vector is 15 min.

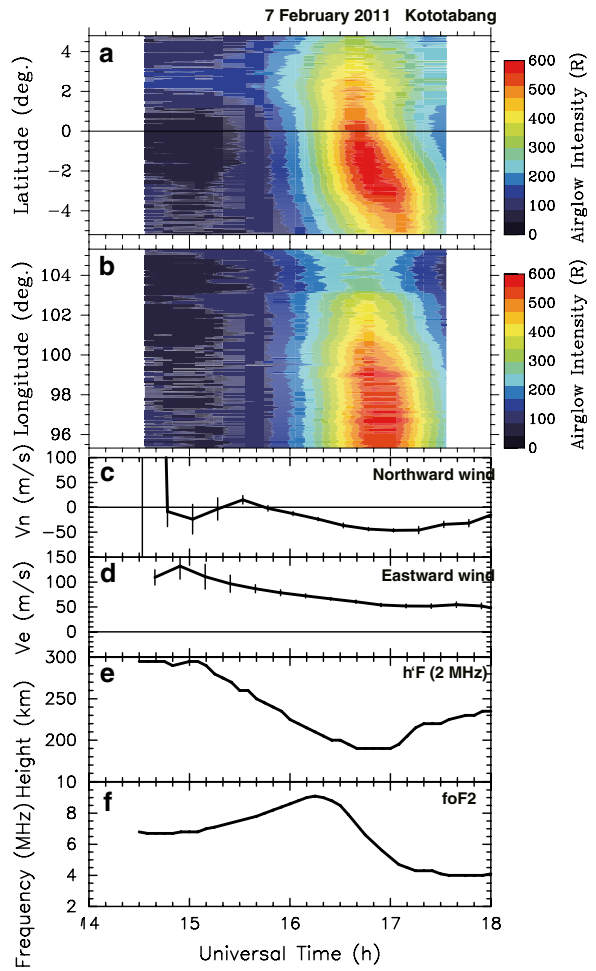

Fig. 5 The 630-nm **a** meridional and **b** zonal keograms represented as absolute airglow intensity, averages and standard deviations of **c** northward and **d** eastward neutral wind velocities observed by an FPI, **e** virtual heights at a frequency of 2 MHz ($h'F$) and **f** F2-region critical frequency (f_oF_2) observed by an ionosonde, at Kototabang on February 7, 2011

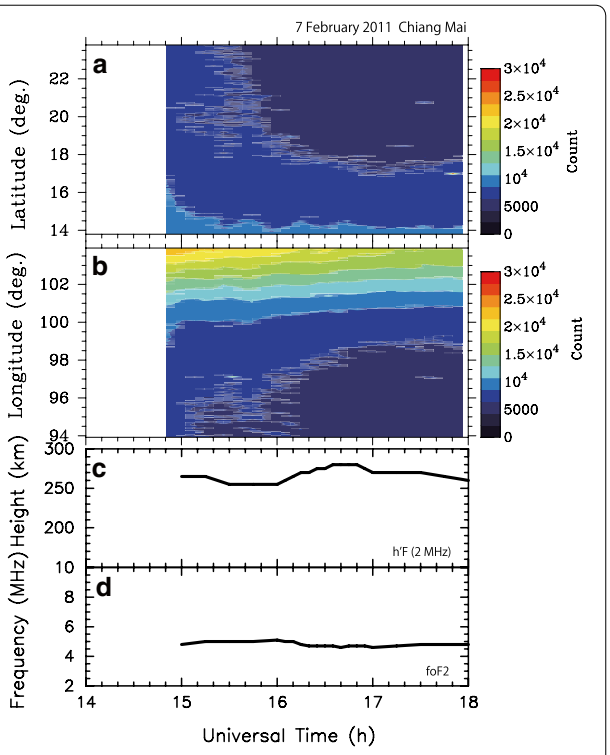

Fig. 6 The 630-nm **a** meridional and **b** zonal keograms represented as raw CCD counts, **c** $h'F$ and **d** f_oF_2 observed by an ionosonde, at Chiang Mai on February 7, 2011

Figure 5c, d shows the northward and eastward thermospheric wind velocities, respectively, observed by the FPI at Kototabang on February 7, 2011. Unfortunately, the FPI operation at Chiang Mai was stopped on this night. The mean values measured from ten fringes of the Kototabang data are plotted with error bars showing standard deviations. The error bars before 1530 UT are significantly large, because the airglow intensity was weak before 1530 UT. Both eastward and northward wind velocities are determined with small error bars after 1530 UT. The northward wind velocity started to decrease and turned southward after 1530 UT in Fig. 5c. The southward wind velocity reached a maximum of ∼ 50 m/s between 1650 and 1720 UT when the MBW was observed in the 630-nm images. The eastward wind velocity was 50–90 m/s and gradually decreased after 1530 UT. The wind direction was approximately eastward before the appearance of the MBW, and then it turned southeastward when the MBW appeared.

We also measured the ionospheric virtual heights by using ionosondes installed at Kototabang and Chiang Mai. These ionosondes are operated by the NICT as the SEALION project (Maruyama et al. 2007). Figures 5e and 6c show the ionospheric virtual heights observed by the ionosondes at Kototabang and Chiang Mai, respectively. These values were obtained from ionograms at a frequency of 2 MHz, which corresponds to a radio frequency reflected at the bottomside F region. The ionospheric virtual height over Kototabang rapidly decreased from 300 km at 1500 UT to 190 km at 1640 UT before and during the airglow enhancement, and it increased from 190 km at 1700 UT to 240 km at 1800 UT after the airglow enhancement. The height was lowest when the airglow intensity reached a maximum between 1640 and 1700 UT. However, at Chiang Mai, the height increased slightly from 250 km at 1600 UT to 280 km at 1640 UT when the MBW was observed at Kototabang.

Figures 5f and 6d show the F2-region critical frequency (f_oF_2) observed by the ionosondes at Kototabang and

Chiang Mai, respectively. These frequencies obtained from ionograms correspond to the plasma density at the F2-region peak. The value of f_oF_2 at Kototabang gradually increased before 1620 UT and rapidly decreased between 1620 and 1720 UT. The decrease of the observed f_oF_2 coincides with the MBW passage. However, clear f_oF_2 variation was not seen at Chiang Mai.

Discussion

We observed the wave-like airglow enhancement, probably corresponding to an MBW, at Kototabang, Indonesia (GLAT: 0.2°S; and MLAT: 10.0°S), which propagated south-southwestward (geomagnetically poleward) with a horizontal velocity of ~290 m/s. This wave was observed from 1540 to 1730 UT (2240–0030 LT) in the local midnight sector. The airglow intensity inside the MBW was 200-600 R, which was much larger than the background 630-nm airglow intensity before the MBW appeared. The observed wave was considered as an MBW, because it has just one phase front moving poleward around midnight. The phase velocity of the present MBW is similar to that observed in Peru (Colerico et al. 1996) and Puerto Rico (Mendillo et al. 1997).

The airglow observation was also conducted at Chiang Mai, Thailand (GLAT: 18.8°N; and MLAT: 8.9°N), which is near the geomagnetically conjugate point of Kototabang. A similar wave-like airglow enhancement was not observed at Chiang Mai when the MBW was observed at Kototabang. This is the first evidence that the MBW does not have geomagnetic conjugacy. This is different from MSTIDs and plasma bubbles, which show clear geomagnetic conjugacy (e.g., Otsuka et al. 2002, 2004).

The airglow enhancement of MBW observed at Kototabang is caused by the ionospheric height decrease, as shown by the ionosonde observation in Fig. 6. The possible mechanisms that cause the height decrease of the ionosphere are downward $\mathbf{E} \times \mathbf{B}$ drift and poleward thermospheric winds. If the observed airglow enhancement was caused by the downward $\mathbf{E} \times \mathbf{B}$ drift, the electric field would be instantly projected onto the northern hemisphere along the geomagnetic field line. As a result, a similar ionospheric height decrease and airglow enhancement should be observed in the northern hemisphere. However, the observed MBW does not exhibit geomagnetic conjugacy. Thus, the MBW and associated ionospheric height decrease are not caused by the electric field.

In the midnight sector at Kototabang, the meridional wind observed by the FPI tends to be northward (geomagnetically equatorward). However, in the present event, the meridional neutral wind at Kototabang turned southward (geomagnetically poleward) after 1540 UT. This poleward wind may be caused by the pressure increase inside the MTM region (e.g., Herrero and Meriwether 1980; Colerico et al. 1996). Both the poleward wind and the gravitational diffusion make the ionospheric plasma move downward along the geomagnetic field line. As the result, the ionospheric height decreases rapidly and the 630-nm airglow intensity increases. These features of poleward wind enhancement and 630-nm airglow enhancement are consistent with the MBW event reported by Otsuka et al. (2003).

The f_oF_2 frequency observed at Kototabang gradually increased from 1500 to 1620 UT, which coincides with the height decrease observed from 1500 to 1640 UT. This relationship between the ionospheric height decrease and the f_oF_2 frequency increase may be caused by an increase in the poleward neutral winds at higher altitudes by the plasma being pushed down along the geomagnetic field line and being temporary accumulated at lower altitudes (e.g., Shiokawa et al. 2002). When the ionospheric height was at a minimum between 1640 and 1700 UT, f_oF_2 decreased rapidly. This decrease in f_oF_2 after 1620 UT is probably caused by the decrease in the plasma density at the F-region peak due to recombination with the high-density neutrals at lower altitudes.

The present observation of the no geomagnetic conjugacy of MBW is consistent with the idea that the MBW is caused by poleward neutral wind enhancement, since the neutral wind is not necessary to have geomagnetic conjugacy. If this poleward neutral wind enhancement was caused by MTM in the equatorial region, the present observation also indicates that this poleward neutral wind is not generated symmetrically to both hemispheres, but only to the southern hemisphere for this case. If the dynamical energy release from the pressure bulge at MTM at the equator caused the poleward neutral wind, it can cause the wind enhancements to both hemispheres. The dynamical energy release may be controlled by some hemispherically asymmetric forces, which may be the asymmetric diurnal tides.

Since this event was observed in the southern-hemispheric summer in February 7, 2011, the dayside subsolar point (maximum solar heating of the thermosphere) occurs in the southern hemisphere. Then, the midnight accumulation point of winds by thermospheric diurnal tide (and associated MTM) would occur in the northern hemispheric side of the geographic equator. This is consistent with the present observation that the MBW propagated southward at Kototabang (geographic equator at 0.2°S). If the MTM occurs at latitudes around Chiang Mai (geographic latitude: 18.8°N), we would not see the MBW at Chiang Mai. If the nighttime equatorward wind by diurnal tide is stronger in the northern hemisphere, the MBW may be launched from MTM only to the southern hemisphere. Maruyama et al. (2008) indicated

that transequatorial winds with 6 h to semidiurnal and diurnal variation also occur in addition to the convergence of the meridional wind.

When the MBW was observed at Kototabang, a small increase in the ionospheric height was observed at Chiang Mai by a co-located ionosonde (Fig. 6c). Unfortunately, we do not know the thermospheric neutral wind variation at Chiang Mai on this night, because FPI was not operating. Poleward winds rapidly cause ionospheric height decreases, and equatorward winds push the plasma to higher altitudes until it balances the downward gravitational diffusion. Thus, a small increase in the equatorward wind may explain the small height increase observed at Chiang Mai. However, if this is the case, it is difficult to explain why the height increase at Chiang Mai was coincident with the MBW at Kototabang. In the remaining part of this section, we discuss another possible generation mechanism for the small height increase in the ionosphere observed at Chiang Mai by the polarization electric field associated with the MBW.

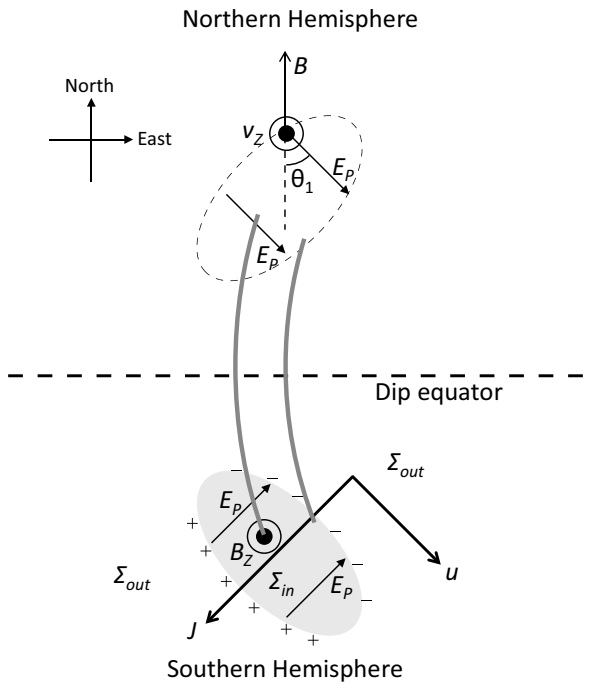

Fig. 7 A schematic picture of the possible ionospheric variations during the MBW event on February 7, 2011. *u* is the thermospheric neutral winds at Kototabang, *J* is an ionospheric current, E_P is a polarization electric field, B_Z and *B* are the vertical and total components of the geomagnetic field, respectively, v_Z is an upward $\mathbf{E} \times \mathbf{B}$ drift, and Σ_{in} and Σ_{out} are height-integrated Pedersen conductivities inside and outside MBW, respectively. We suggest that the polarization electric field inside the observed midnight brightness wave in the southern hemisphere is projected to the northern hemisphere, causing the observed ionospheric height increase in the northern hemisphere

Figure 7 shows the schematic picture of the possible electromagnetic coupling of the two hemispheres during the present MBW event. The thermospheric neutral wind, **u**, was approximately southeastward at Kototabang when the MBW was observed, as shown by the FPI data in Fig. 5c, d. The neutral wind drives the ionospheric current, **J**, which has a direction of $\mathbf{E} + \mathbf{u} \times \mathbf{B}$, where **B** is the geomagnetic field vector. The background electric field, **E**, is assumed to be negligible, considering that the speed of the background F-layer height decrease at 15–16 UT in Fig. 6c (~4 m/s) is smaller than the subsequent F-layer height raise (12.5 m/s). Thus, the horizontal current flows southwestward due to the southeastward **u**. The Pedersen conductivity inside the MBW is larger than that outside the MBW, because the Pedersen conductivity is proportional to the product of both the plasma and neutral densities and thus to the 630-nm airglow intensity. Considering the current flows across the MBW, positive and negative space charges would be accumulated at the southern and northern boundaries of the MBW, respectively, because of the spatial inhomogeneity of the Pedersen conductivity and to maintain the current continuity inside and outside the MBW. Because of this space charge, a polarization electric field, E_P, is generated anti-parallel to the current (northeastward).

This polarization electric field will be projected onto the northern hemisphere along the geomagnetic field line almost without attenuation. The projected electric field is southeastward. The eastward component of the electric field and northward component of the geomagnetic field generate upward $\mathbf{E} \times \mathbf{B}$ drift. This could explain why a small height increase was observed at Chiang Mai simultaneously with the MBW at Kototabang. The start of the MBW at Kototabang was at 1530 UT. At this timing, the F-layer height decrease was stopped at Chiang Mai. Then, it turned to increase at 1600 UT.

According to this scenario, we roughly estimate the value of the upward $\mathbf{E} \times \mathbf{B}$ drift in the northern hemisphere. The upward $\mathbf{E} \times \mathbf{B}$ drift velocity, v_Z, in the northern hemisphere is expressed by the eastward component of the projected polarization electric field and the northward component of the geomagnetic field as

$$v_Z = \frac{E_P \sin\theta_1 \cos I}{B} = \left(1 - \frac{\Sigma_{out}}{\Sigma_{in}}\right) u \frac{B_Z}{B} \sin\theta_1 \cos I, \quad (1)$$

where Σ_{in} and Σ_{out} are the height-integrated Pedersen conductivities inside and outside the MBW, respectively, *B* is the geomagnetic field intensity at Chiang Mai, θ_1 is an angle formed by the direction of the projected polarization electric field and the south, and *I* is the magnetic dip angle.

The height-integrated Pedersen conductivity, Σ_{in} and Σ_{out}, is nearly proportional to the 630-nm airglow intensity (e.g., Kelley 2009), therefore, $\Sigma_{out}/\Sigma_{in} = 100(R)/600(R)$. Because the projected polarization electric field is southeastward, the value of θ_1 is ~45°. The B_Z at Kototabang and B at Chiang Mai (conjugate point of Kototabang) are 1.22×10^4 nT and 3.76×10^4 nT at an altitude of 250 km. The value of I is 18.9°. The observed thermospheric neutral winds, u, at Kototabang were ~71 m/s southeastward when the MBW was observed. Substituting these values into Eq. (1), we calculated v_Z as 12.8 m/s. The ionospheric height increase observed at Chiang Mai was ~30 km for 40 min in Fig. 6, giving a vertical velocity of 12.5 m/s. This value is fairly comparable to that from Eq. (1). Thus, we suggest that the observed small height increase over Chiang Mai was caused by the polarization electric field projected from the MBW in the southern hemisphere. This indicates that the electromagnetic coupling between hemispheres can occur even though the original disturbance is caused purely by the neutral wind.

Conclusions

We observed nighttime 630-nm airglow at Kototabang, Indonesia, and Chiang Mai, Thailand, which are nearly geomagnetically conjugate stations at low latitudes (~10° MLAT). An increase in the 630-nm airglow intensity of 200-600 R was observed from 1540 to 1730 UT (2240–0030 LT) on February 7, 2011, at Kototabang. This airglow enhancement is considered to be an MBW, because it was observed around local midnight and propagated geomagnetically poleward only once. The MBW has an ESE-WNW phase front and propagated south-southwestward with a horizontal velocity of ~290 m/s. However, a similar MBW structure was not observed at Chiang Mai, indicating that the observed MBW did not have geomagnetic conjugacy. The meridional neutral wind observed by the FPI increased from −20 m/s (northward) to 50 m/s (southward), and the ionospheric virtual height observed by the ionosonde at Kototabang decreased from 300 to 190 km when the MBW was observed. This southward wind is probably generated by the pressure increase inside the MTM. We suggest that the airglow enhancement observed as an MBW was caused by the southward (poleward) neutral wind moving the plasma down to lower altitudes. The present observations also imply that this poleward neutral wind is not generated symmetrically to both hemispheres, but only to the southern hemisphere, possibly because of asymmetric diurnal tide. When the MBW was observed at Kototabang, the ionospheric height increased slightly at Chiang Mai, by ~30 km. We suggest that the polarization electric field projected from the MBW in the southern hemisphere generated upward $\mathbf{E} \times \mathbf{B}$ drift in the northern hemisphere at Chiang Mai, showing electromagnetic coupling between hemispheres can occur even though the original disturbance is caused purely by the neutral wind.

Authors' contributions

DF has carried out the main data analysis and wrote the manuscript during his Ph.D. course in Nagoya University. KS supervised the study and improved the manuscript as the Principal Investigator of the OMTIs and the supervisor of DF. YO helped to carry out the operation of the airglow imagers and FPIs used in this paper and improved the interpretation of the results. MK, TY, and MN carried out the operation of the NICT ionosondes at Chiang Mai and Kototabang and improved the interpretation of the results. SK managed the operation of the airglow imager and the FPI at Chiang Mai, Thailand. CYY managed the operation of the instruments at Kototabang, Indonesia. All authors read and approved the final manuscript.

Author details

[1] Institute for Space-Earth Environmental Research, Nagoya University, Nagoya, Aichi 464-8601, Japan. [2] National Institute of Information and Communications Technology, Koganei, Tokyo 184-8795, Japan. [3] Department of Physics and Materials Science, Faculty of Science, Chiang Mai University, Chiang Mai 50200, Thailand. [4] Indonesian National Institute of Aeronautics and Space (LAPAN), Bandung 40173, Indonesia. [5] Murata Machinery Co. Ltd., Inuyama, Japan.

Acknowledgements

We thank Y. Katoh, M. Satoh, Y. Yamamoto, and Y. Hamaguchi of the Institute for Space-Earth Environmental Research (ISEE), Nagoya University, for their helpful support in the development and operation of the optical instruments of ISEE. The airglow observation at Kototabang was conducted in collaboration with the Research Institute for Sustainable Humanosphere, Kyoto University, Japan, and the National Institute of Aeronautics and Space (LAPAN), Indonesia. The airglow observation at Chiang Mai and the ionosonde observations at Kototabang and Chiang Mai were performed by the National Institute of Information and Communications Technology (NICT), Japan, as part of the SEALION project. The airglow observation at Chiang Mai was conducted in cooperation with Chiang Mai University, NICT, and ISEE. All the data of airglow images and winds from the Fabry–Perot interferometer used in this paper are available at ISEE, Nagoya University. The ionosonde data are available at NICT. This work was supported by Grants-in-Aid for Scientific Research (13573006, 20244080, 15H05815, and Priority Area 764), by Strategic Funds for the Promotion of Science and Technology (IUGONET), from the Ministry of Education, Culture, Sports, Science and Technology, Japan, and by JSPS Core-to-Core Program, B. Asia-Africa Science Platforms.

Competing interests

The authors declare that they have no competing interests.

Publisher's Note

Received: 4 January 2017 Accepted: 31 July 2017
Published online: 15 August 2017

References

Colerico M, Mendillo M, Nottingham D, Baumgardner J, Meriwether J, Mirick J, Reinisch BW, Scali JL, Fesen CG, Biondi MA (1996) Coordinated measurements of F region dynamic related to the thermospheric midnight temperature maximum. J Geophys Res 101:26783–26793

Finlay CC et al (2010) International geomagnetic reference field: the eleventh generation. Geophys J Int 183:1216–1230. doi:10.1111/j.1365-246X.2010.04804.x

Fukushima D, Shiokawa K, Otsuka Y, Ogawa T (2012) Observation of equatorial nighttime medium-scale traveling ionospheric disturbances in 630-nm airglow images over 7 years. J Geophys Res 117:A10324. doi:10.1029/2012JA017758

Fukushima D, Shiokawa K, Otsuka Y, Nishioka M, Kubota M, Tsugawa T, Nagatsuma T, Komonjinda S, Yatini CY (2015) Geomagnetically conjugate observation of plasma bubbles and thermospheric neutral winds at low latitudes. J Geophys Res. doi:10.1002/2014JA020398

Greenspan JA (1966) Synoptic description of the 6300 Å nightglow near 78° west longitude. J Atmos Terr Phys 28:739–745

Herrero FA, Meriwether JW (1980) 6300-Å airglow meridional intensity gradients. J Geophys Res 85:4194–4204

Hunsucker RD (1982) Atmospheric gravity waves generated in the high-latitude ionosphere: a review. Rev Geophys Space Phys 20:293–315

Kelley M (2009) The earth's ionosphere: plasma physics and electrodynamics, 2nd edn. Academic Press, Cambridge ISBN:9780120884254

Kubota M, Ishii M, Tsugawa T, Uemoto J, Jin H, Otsuka Y, Shiokawa K (2009) New observational deployments for SEALION—airglow measurements using all-sky imagers. J Natl Inst Inf Commun Technol 56(1–4):299–307

Maruyama T, Saito S, Kawamura M, Nozaki K (2008) Thermospheric meridional winds as deduced from ionosonde chain at low and equatorial latitudes and their connection with midnight temperature maximum. J Geophys Res 113:A09316. doi:10.1029/2008JA013031

Martinis C, Hickey D, Oliver W, Aponte N, Brum CGM, Akmaev R, Wright A, Miller C (2013) The midnight temperature maximum from Arecibo incoherent scatter radar ion temperature measurements. J Atmos Sol Terr Phys 103:129–137. doi:10.1016/j.jastp.2013.04.014

Maruyama T, Kawamura M, Saito S, Nozaki K, Kato H, Hemmakorn N, Boonchuk T, Komolmis T, Ha Duyen C (2007) Low latitude ionosphere-thermosphere dynamics studies with inosonde chain in Southeast Asia. Ann Geophys 25(7):1569–1577

Mayr HG, Harris I, Spencer NW, Hedin AE, Wharton LE, Porter HS, Walker JCG, Carlson HC Jr (1979) Tides and the midnight temperature anomaly in the thermosphere. Geophys Res Lett 6:447–450

Mendillo M, Baumgardner J, Nottingham D, Aarons J, Reinisch B, Scali J, Kelley M (1997) Investigations of thermospheric-ionospheric dynamics with 6300-Å images from the Arecibo Observatory. J Geophys Res 102(A4):7331–7343. doi:10.1029/96JA02786

Nelson GJ, Cogger LL (1971) Dynamical behavior of the nighttime ionosphere at Arecibo. J Atmos Terr Phys 33:1711–1726

Otsuka Y, Shiokawa K, Ogawa T, Wilkinson P (2002) Geomagnetic conjugate observations of equatorial airglow depletions. Geophys Res Lett 29(15):1753. doi:10.1029/2002GL015347

Otsuka Y, Kadota T, Shiokawa K, Ogawa T, Kawamura S, Fukao S, Zhang S-R (2003) Optical and radio measurements of a 630-nm airglow enhancement over Japan on 9 September 1999. J Geophys Res 102(A6):1252. doi:10.1029/2002JA009594

Otsuka Y, Shiokawa K, Ogawa T (2004) Geomagnetic conjugate observations of medium-scale traveling ionospheric disturbances at midlatitude using all-sky airglow imagers. Geophys Res Lett 31(15):L15803. doi:10.1029/2004GL020262

Shiokawa K, Katoh Y, Satoh M, Ejiri MK, Ogawa T, Nakamura T, Tsuda T, Wiens RH (1999) Development of optical mesosphere thermosphere imagers (OMTI). Earth Planets Space 51(7–8):887–896. doi:10.1186/BF03353247

Shiokawa K, Katoh Y, Satoh M, Ejiri MK, Ogawa T (2000) Integrating-sphere calibration of all-sky cameras for nightglow measurements. Adv Space Res 26:1025–1028

Shiokawa K, Otsuka Y, Ogawa T, Balan N, Igarashi K, Ridley AJ, Knipp DJ, Saito A, Yumoto K (2002) A large-scale traveling ionospheric disturbance during the magnetic storm of 15 September 1999. J Geophys Res 107(A6):1088. doi:10.1029/2001JA000245

Shiokawa K, Otsuka Y, Ogawa T, Wilkinson P (2004) Time evolution of high-altitude plasma bubbles imaged at geomagnetic conjugate points. Ann Geophys 22(9):3137–3143

Shiokawa K, Otsuka Y, Ogawa T (2009) Propagation characteristics of nighttime mesospheric and thermospheric waves observed by optical mesosphere thermosphere imagers at middle and low latitudes. Earth Planets Space 61(4):479–491. doi:10.1186/BF03353165

Shiokawa K, Mori M, Otsuka Y, Oyama S, Nozawa S (2012a) Motion of high-latitude nighttime medium-scale traveling ionospheric disturbances associated with auroral brightening. J Geophys Res 117:A10316. doi:10.1029/2012JA017928

Shiokawa K, Otsuka Y, Oyama S, Nozawa S, Satoh M, Katoh Y, Hamaguchi Y, Yamamoto Y, Meriwether J (2012b) Development of low-cost sky-scanning Fabry–Perot interferometers for airglow and auroral studies. Earth Planets Space 64(11):1033–1046. doi:10.5047/eps.2012.05.004

Sobral JHA, Takahashi H, Abdu MA, Muralikrishna P, Sahai Y, Zamlutti CJ, de Paula ER, Batista PP (1993) Determination of the quenching rate of the $O(^1D)$ by $O(^3P)$ from rocket-borne optical (630 nm) and electron density data. J Geophys Res 98(A5):7791–7798. doi:10.1029/92JA01839

Yamamoto M-Y, Kubota M, Takeshita S, Ishii M, Murayama Y, Ejiri M (2002) Calibration of CRL all-sky imagers using an integrating sphere. Adv Polar Upper Atmos Res 16:173–180